Journal of Sustainable Metallurgy (2022) 8:1590–1605
https://doi.org/10.1007/s40831-022-00581-1

RESEARCH ARTICLE

Effect of B_2O_3 on the Liquidus Temperature and Phase Equilibria in the $CaO–Al_2O_3–SiO_2–B_2O_3$ Slag System, Relevant to the Smelting of E-waste

Md Khairul Islam[1,2,4] · Mark I. Pownceby[2] · Michael Somerville[2] · James Tardio[1] · Nawshad Haque[3] · Suresh Bhargava[1]

Received: 25 May 2022 / Accepted: 9 August 2022 / Published online: 12 September 2022

Abstract

The phase equilibria in the $CaO–Al_2O_3–SiO_2$ ternary system doped with around 5, 10, 15 and 20 wt% B_2O_3 was studied using a high-temperature equilibration followed by rapid quenching technique. Fifteen samples with CaO/SiO_2 (C/S) ratios of 0.3, 0.6 and 1.0 containing 15.6–19.1 wt% Al_2O_3 were equilibrated at a range of temperatures close to predicted liquidus phase boundaries within the B_2O_3-free ternary. Quenched samples were characterised using Scanning Electron Microscopy (SEM) to reveal the equilibrium phase assemblage and Electron Probe Microanalysis (EPMA) to determine the chemistry of individual phases. The liquidus temperatures of the synthetic slags were determined within an uncertainty of ± 10–20 °C. Depending on temperature and composition, anorthite ($CaO.Al_2O_3.2SiO_2$), pseudowollastonite ($CaO.SiO_2$), gehlenite ($2CaO.Al_2O_3.SiO_2$) and tridymite (SiO_2) crystals were observed in equilibrium with the liquid phase at temperatures below the liquidus. Doping with successively higher amounts of B_2O_3 caused the boundaries of the initial primary phase fields to shift position, generally resulting in a reduction of the liquidus temperature. The lowest liquidus temperature was 900 °C for slag with initial composition having C/S = 0.6 and 18.8 wt% B_2O_3 representing a decline of the liquidus by 435 °C compared to the undoped slag. Only one sample (C/S = 1.0, 18.8 wt% B_2O_3) resulted in an increase in the liquidus temperature due to the expansion of the pseudowollastonite phase field at high B_2O_3 contents. Based on the experimental results, B_2O_3 may be a suitable fluxing agent to reduce the smelting temperature in the $CaO–Al_2O_3–SiO_2–B_2O_3$ quaternary system. A comparison of results with liquidus data for similar experiments using Na_2O flux showed that B_2O_3 was more effective in lowering the liquidus.

The contributing editor for this article was Sharif Jahanshahi.

✉ Md Khairul Islam
Khairul.islam@csiro.au

[1] Centre for Advanced Materials & Industrial Chemistry (CAMIC), School of Science, RMIT University, GPO Box 2476, Melbourne, VIC 3001, Australia

[2] CSIRO Mineral Resources, Private Bag 10, Clayton South, VIC 3169, Australia

[3] CSIRO Energy, Private Bag 10, Clayton South, VIC 3169, Australia

[4] Bangladesh Council of Scientific and Industrial Research (BCSIR), IMMM, Joypurhat 5900, Bangladesh

Graphical Abstract

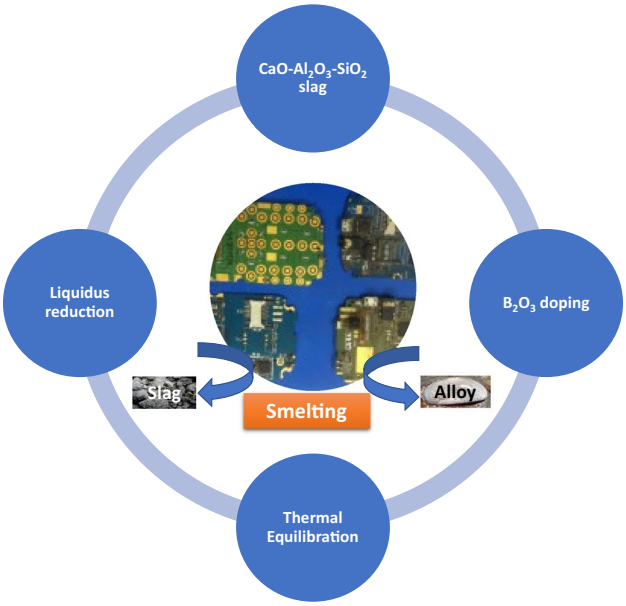

Keywords PCBs · B_2O_3 doping · Smelting · E-waste · Phase equilibria · Slags · Liquidus

Introduction

The gradual depletion of essential minerals and metal primary deposits, combined with the possible interruption of critical metals supplies due to geopolitical situations, make it challenging for electronics industries to maintain or increase future supplies. For instance, according to the Royal Society of Chemistry, smartphones contain around 30 different elements and among these, six are currently in scarce supply and are estimated to exhaust their natural sources within the next 100 years based on the assumptions of current use rate and the available global reserves [1]. Considering these circumstances, increased recycling to recover the embedded high-value, scarce materials from end-of-life (EoL) electronics is an obvious way to ensure future availability. Approximately 53.6 million metric tonnes (Mt) of electronic waste (e-waste) from multiple waste streams was generated across the world in 2019, however, the collection and recycling of only 17% of the available e-waste was reported [2]. The amount of e-waste generation is projected to rise to 70.4 Mt by the year 2030 [2]. In many devices, the concentration of several precious metals (Ag, Au, Pt) and base metals (Cu, Sn, Ni) are significantly higher than in their primary mined ores that are currently processed to extract the metals [3, 4]. Recycling of these metals from secondary resources therefore has multiple benefits such as reducing the carbon emissions associated with new exploration and mining and with the subsequent processing steps which are typically highly energy intensive [5, 6]. Moreover, recycling protects the environment from the potentially harmful effects that result from dumping and landfilling of the rapidly growing e-waste [7].

The major embedded metal values in e-waste materials are present in complex printed circuit boards (PCBs) as plastic-ceramic–metal composites [8–11]. Several processing routes including physical separation, pyrometallurgical, hydrometallurgical, biohydrometallurgical and supercritical techniques, either individually or in combination, have been proposed and have been extensively investigated to extract value metals from PCBs [12, 13]. However, still there remains significant challenges to recover values at an industrial scale primarily because of the heterogeneity of the materials, the rapid changing of technology and the chemistry and structure of the materials. Pyrometallurgical processing is, therefore, becoming the preferred method for many commercial operations and is currently being adapted by several industries across the world including Umicore, Outotec, and Glencore [14]. In these smelters/refiners, e-waste scrap is co-fed with ores and other wastes, in particular those coming from Cu smelting industries. However, many countries do not have primary Cu smelters and in some large countries with smaller populations such as Australia that have smelters located far from the population centres, additional costs are incurred to collect and transport materials to the remote smelter [15]. In those circumstances, a relatively smaller scale smelting process would be a suitable

alternative in the beneficiation of most metals within the alloy stream. The metal-poor slag generated during the smelting of PCBs contains mostly SiO_2, Al_2O_3 and CaO with some other minor oxides [16–18]. These three major oxides make the slag system highly refractory requiring high operating temperatures to completely melt the PCBs and allow the separation of the metals from the slag. The high operating temperatures (typically > 1400 °C) may cause difficulties in keeping control of the process and the addition of a suitable flux could potentially reduce the liquidus temperature of the slags generated and make the process operationally viable at a significantly lower temperature. This in turn reduces the energy required to recover the metals from e-waste thereby lowering emissions.

Investigations into the phase equilibria of complex liquid oxide systems have been conducted for many years, particularly in relation to the formation of primary igneous rock types [19]. Similarly, research to investigate metallurgical operations, especially in slag-bearing systems relevant to the smelting of high-value metals such as copper and lead, have also been extensive [20–22]. This has led to an increased understanding of the partitioning of metals between solids and liquids in the relevant systems as well as improvements in the design of the types of refractory materials used in metal processing and production. In particular, several studies have focussed on improving the mould flux for continuous casting of steels from blast furnace slags in the $CaO–Al_2O_3–SiO_2–MgO$ system [23, 24]. Since commercial mould fluxes contain around 2–15% CaF_2 the introduction of molten liquids releases fluorine which is detrimental to the equipment and creates environmental hazards. Based on these studies steps have been taken to replace CaF_2 with other fluxes such as B_2O_3 [25, 26]. These types of studies have also been important in glass technology industries though they essentially only discuss the physical, mechanical, optical and some electrical properties of glasses rather than the phase equilibria of the systems [27, 28]. The last example involves research in the energy industry where many researchers studied the phase equilibria of aluminosilicate systems, specifically focusing on coal gasification, ash fusibility and viscosity of slags derived from coal ash [29–31]. While the study of phase equilibria in slag systems has previously been applied to several areas, a new emerging area is in the application of existing knowledge of phase equilibria data or the development of new slag systems which could potentially apply to the smelting of discarded PCBs at a moderately low temperature to assist in the separation of metal and slag phases and hence increase the recovery of valuable components from existing (at present) waste streams.

Since the $CaO–Al_2O_3–SiO_2$ (CAS) slag system generated during the pyrometallurgical processing of e-waste PCBs needs elevated temperatures, the addition of a suitable metal oxide fluxing agent could be a way to reduce the liquidus temperature. For example, the effect of minor elements such as TiO_2, MnO, Na_2O, K_2O, CaS, and B_2O_3 on the liquidus temperatures of blast furnace slags was previously investigated by Chen and co-workers [32]. In experiments within the melilite primary phase field, it was shown that the decrease in liquidus temperature, depended on the addition of particular oxides. The strongest effect on liquidus temperature was by B_2O_3 where the liquidus was reduced by 136 °C due to fluxing with 4.9 wt% B_2O_3. However, this study only reported data from a limited composition range (up to 4.9 wt% B_2O_3) and only within one master slag composition relevant to blast furnace ironmaking i.e., the $SiO_2–Al_2O_3–CaO–MgO$ system. It is not clear how the liquidus changes with further B_2O_3 addition.

The structure and viscosity of slags in the $CaO–SiO_2–Al_2O_3–B_2O_3$ system was also investigated for applications in ironmaking (blast furnace slags) and as a mould flux for continuous casting of steel [25]. Similarly, the conductivity, heat transfer capability, fluidity, and crystallization behaviour have been studied thoroughly [33–35]. Further studies have focussed on the physical and mechanical properties of the glass (quenched slag) phase. B_2O_3 can act as an amphoteric oxide and also as an aluminosilicate network modifier by reducing the relative number of strong bonds in the glass and lowering the melting point and viscosity [36–38]. Wang et al. [39] investigated melting properties (i.e., softening, hemispherical and fluidity temperatures) in the $CaO–SiO_2–Al_2O_3–B_2O_3$ system with 5–9 wt% B_2O_3 and a C/S ratio ranging from 0.83 to 1.5. While boron did not change the hemispherical temperature (temperature at which cylindrical flux sample loses its 50% height during hot stage microscopy technique), the viscosity decreased significantly with increasing B_2O_3. While it is possible to retain B_2O_3 in the slag originating from the boron-based flame retardants in PCBs, to the best of our knowledge the study of phase equilibria in $CaO–Al_2O_3–SiO_2–B_2O_3$ slags relevant to e-waste smelting has not been reported so far.

Experimental

Materials

Three ternary master slags based on the $CaO–Al_2O_3–SiO_2$ slag system were prepared by melting reagent grade $CaCO_3$ (99.5 wt%, Sigma-Aldrich), Al_2O_3 (99.5 wt%, VWR Chemicals), and SiO_2, (99.9 wt%, Sigma-Aldrich) at 1600 °C in air, at conditions well above the liquidus temperature to ensure complete melting and homogenization of all components [40]. Compositions with CaO/SiO_2 (C/S) ratios of 0.3 (series S100), 0.6 (S200) and 1.0 (S300) were prepared, each with an Al_2O_3 content close to 20 wt%. A platinum crucible was

used to hold the materials during melting inside a muffle furnace and for each master slag composition a transparent, glassy state of the quenched pre-melted slags was obtained. B_2O_3 (99.95wt%, VWR Chemicals) was then added, nominally at levels of 5, 10, 15 and 20 wt% B_2O_3 to each of the three master slags producing twelve B-doped sub-slag compositions in total. Note, that while the C/S ratio of the quaternary sub-slags were kept the same, the percentage of Al_2O_3 component decreased proportionally due to the addition of B_2O_3 (Table 1). The pre-cursor, B-doped sub-slag compositions were then re-melted at 1600 °C, quenched and pulverised to obtain powdered samples that were then screened to < 212 µm in particle size. Platinum foil used for containing the sub-slags in the drop quench experiments was supplied by Cookson Dental, UK.

Composition of the Pre-melted Slags

X-ray Fluorescence Spectroscopy (XRF) and Inductively Coupled Plasma Optical Emission Spectrometry (ICP-OES) were used to analyse the compositions of the three master slags (S100, S200 and S300) and the twelve B_2O_3-doped sub-slags. For the XRF measurements, the slag samples were fused with lithium borate to produce a homogenous glass disc to analyse in the XRF instrument (Bruker 4 kW S8 Tiger WDXRF). The measurement accuracy of the XRF results was close to 0.5% relative, based on calibration datasets collected by CSIRO over several years. Since boron is a light element and is difficult to analyse with XRF, a Varian 730-ES ICP-OES was used. To analyse the samples using ICP-OES, the powdered slag samples were digested with HNO_3 and HF and heated until the dissolution was complete.

Table 1 Compositions of the investigated master slags S100, S200 and S300 and the twelve B-doped sub-slags

Sample ID	Al_2O_3 (%)	CaO (%)	SiO_2 (%)	B_2O_3 (%)	C/S ratio
S100	18.7	20.0	61.1	0.0	0.3
S105B	18.2	19.4	57.3	5.2	0.3
S110B	17.5	18.5	54.9	9.2	0.3
S115B	16.5	17.5	51.9	14.1	0.3
S120B	15.6	16.5	48.9	19.0	0.3
S200	19.1	29.6	51.0	0.0	0.6
S205B	18.5	28.8	47.9	4.8	0.6
S210B	17.6	27.2	45.5	9.7	0.6
S215B	16.7	25.9	43.3	14.1	0.6
S220B	15.8	24.5	40.9	18.8	0.6
S300	19.1	39.5	41.0	0.0	1.0
S305B	18.2	38.0	38.6	5.2	1.0
S310B	17.4	36.3	36.7	9.7	1.0
S315B	16.3	34.2	34.6	14.9	1.0
S320B	15.6	32.4	33.2	18.8	1.0

Before the analysis with ICP-OES the samples were diluted as required. Certified multi-element standards were used to check the accuracy of the calibrations and analyses. The compositions of the investigated master and sub-slags are shown in Table 1. The resulting compositions were close to the intended target compositions and showed negligible B loss had occurred during melting. Figure 1 shows the composition of the three master slags and their primary phase fields within the $CaO–Al_2O_3–SiO_2$ ternary phase diagram.

Liquidus Determination Experiments

To study the phase equilibria, the prepared slag and B-doped sub-slag powders were equilibrated in air at high temperatures inside a vertical tube furnace. All samples were rapidly quenched in a water bath (room-temperature water) situated at the open bottom end of the furnace. In this way the high temperature structure and phase assemblage of the system was preserved through rapid solidification.

For the liquidus determination experiments, capsules made from thin platinum foil (0.025 mm thickness) were filled with 200–300 mg of the slag mixtures and suspended from the top of a vertical tube furnace by a platinum wire (0.5 mm diameter). The top end of the capsules remained open and exposed to the furnace (air) atmosphere. The capsules were then lowered into a 3–4 cm long hot zone at the centre of the furnace tube. A Type-B thermocouple inserted in an alumina sheath was placed close to the samples to continuously measure the temperature. The thermocouple was calibrated against the melting temperature of pure copper and shown to have an accuracy of ± 5 °C. Both the thermocouple and sample holder were inserted through the top endcap and sealed, while the bottom endcap was closed with a thin polypropylene sheet touching the water surface of the quenching bath. Figure 2a shows a schematic of the furnace arrangement for a drop quench test. A more detailed description of the experimental methods can be found in reference [42].

Based on a procedure developed by Rait [43] the slags were heated to an initial temperature 100 °C above the planned experimental temperature, at a rate of 200 °C/h. The samples were held for 30 min at that temperature to completely melt and homogenize the molten slag. To introduce nucleation sites and thus assist crystallization at equilibrium, the temperature was then reduced to 200 °C below the experimental temperature and held for 30 min before being heated to the final experimental temperature. The samples were allowed to equilibrate for 4–24 h at the experimental temperature to complete the reaction. Once the equilibration time was reached, the samples were released from the top holder to drop directly into the quenching water bath to ensure rapid solidification. The

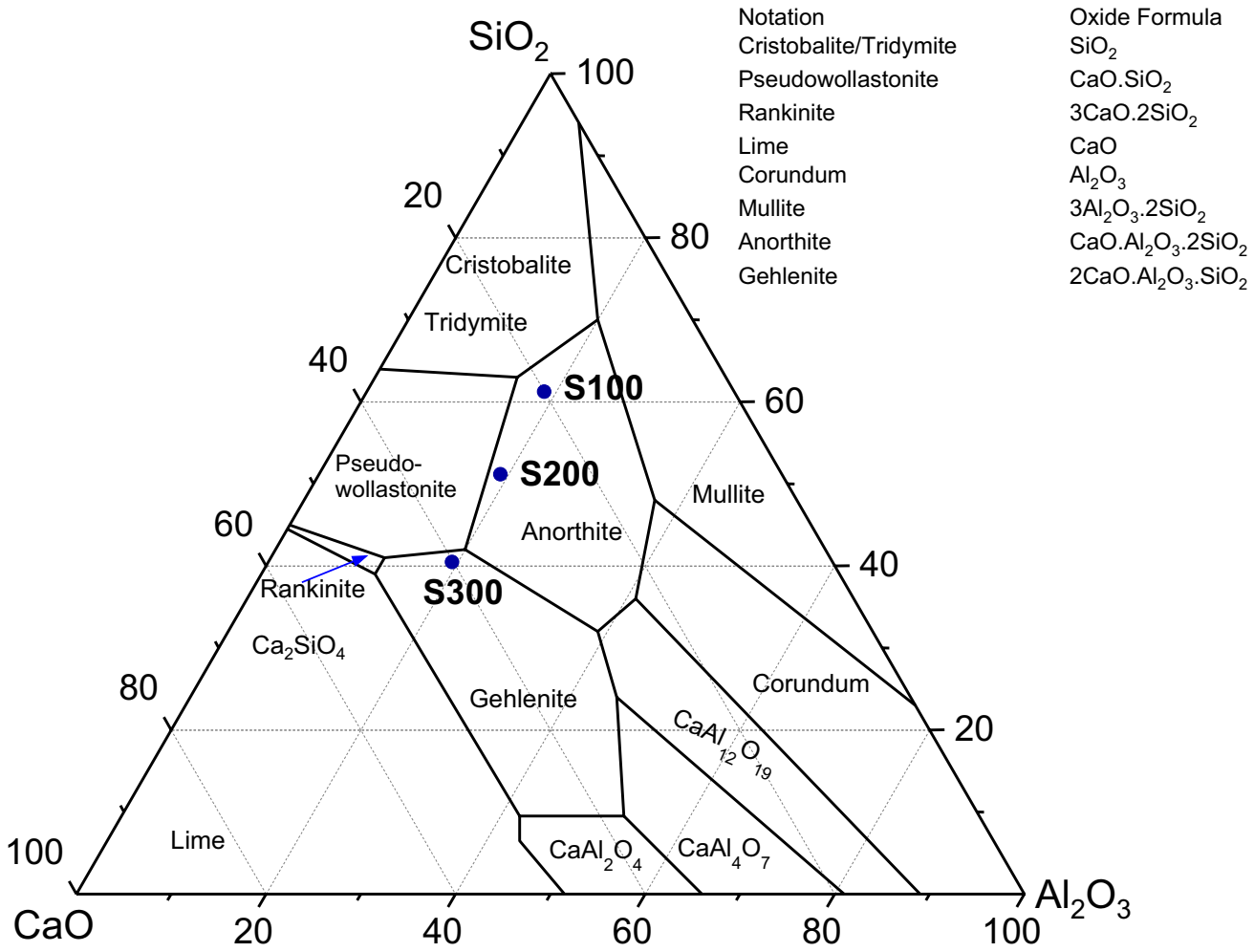

Fig. 1 The ternary CaO-Al_2O_3-SiO_2 slag system showing the location of major phase boundaries and the three master slag compositions; redrawn using data from reference [41]

temperature profile used for the equilibrium drop-quench experiments is shown as Fig. 2b.

The samples obtained from the drop quench tests were dried immediately to avoid any potential water absorption by the phases, separated from the platinum capsules, and then mounted in epoxy resin for analysis. After grinding and polishing of the resin blocks, the specimens were examined using SEM back-scattered electron (BSE) imaging to determine the phase assemblage and the compositions of the phases were qualitatively analysed using EDS and quantitatively using EPMA. Every new experiment was based on the phase assemblage from of the previous test depending on the equilibrium phases present, to determine if a higher or lower temperature was required. Repeat tests were done above the bracketed liquidus to examine if crystals present and below the temperature to check the absence of primary solid phase.

SEM–EDS Analysis

The mounted quenched slag samples were initially ground using SiC abrasive papers, finely polished with diamond suspensions of different particle sizes (6, 3 and 1 μm). Grinding and polishing of samples were performed in water-less medium to avoid dissolution of any phase and used oil/alcohol-based lubricants (i.e. DP-Lubricant Yellow from Struers). Before examination in the SEM the polished samples were carbon coated to avoid charge build up on the surface. An FEI Quanta 400 SEM equipped with a Bruker EDS system was used to investigate the microstructure and identify the phases present. The SEM analysis was performed using an accelerating potential of 15 kV with a working distance of 10.0 mm. EDS was used to measure the preliminary compositions of the solid and/or liquid phases present and hence identify the crystal phases present in the slag samples.

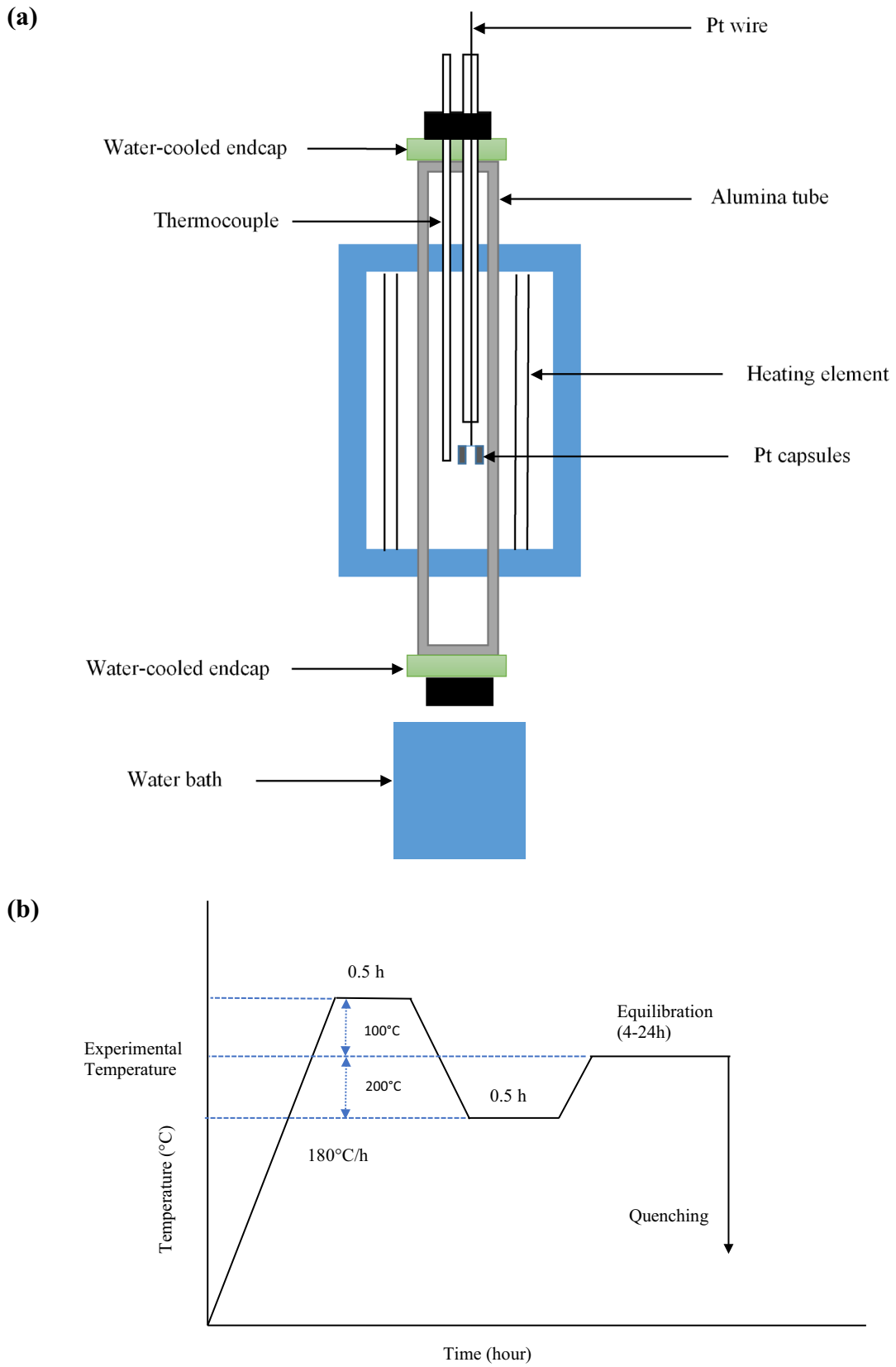

Fig. 2 **a** Schematic diagram of the drop quench test furnace and experimental setup **b** thermal profile used for the equilibrium-quenching experiments (after Rait [43])

Electron Probe Microanalysis (EPMA)

The quantitative analysis of the different equilibrium phases was performed using a JEOL (Model JXA-8500F) electron microprobe. The analysis was performed with an accelerating voltage of 12 kV, a probe current of 10 nA and a beam defocus of 5 µm. The standards used for calibration were wollastonite ($CaO.SiO_2$) for Ca and Si, danburite ($CaB_2Si_2O_8$) for B and spinel ($MgAl_2O_4$) for Al. Caution was taken to minimize loss of boron by evaporation due to the excitement by the electron beam by defocussing the beam and employing short counting times (20 s. on the main B peak and 10 s. on the background). In addition, the low-beam current (10 nA) helped reduce potential volatilization. With this arrangement it was observed that there was negligible boron loss during analysis as confirmed by repeat analyses. Since boron is very sensitive and lighter it requires more rigorous precautions to reduce uncertainty in analysis. Before analysis, all samples were carbon coated together with the standards to ensure a similar coating thickness so that no additional variable can come from the differential coating thickness. For each phase at least 10–15 points were taken, and the average composition was reported.

Equilibrium Time

For most of the drop quench tests, 4 h was allowed for equilibrium to be reached between the liquid and primary crystal phases. This time allowance was confirmed by comparing the phase assemblages and their compositions for samples equilibrated at 4 and 24 h. After 24 h there was no significant difference in the phases present and their compositions from the samples equilibrated for 4 h. For example, the master slag S200 was equilibrated for 4 and 24 h at 1300 °C. Both equilibration times produced a slag system consisting of anorthite as the primary phase and liquid. The measured composition of the anorthite crystals and the liquid phase were the same in each case. In both cases the anorthite crystals and liquid phases proved to be homogeneous through checking compositions at many locations in the samples. In some samples close to eutectic compositions and at lower temperatures, a longer equilibration time of 8 h was used. For these samples the longer equilibration time was used to ensure the precipitation of a primary crystal phase.

Results and Discussion

Phase Relations at Equilibrium

Some representative microstructures of the equilibrium phases are shown in Fig. 3a–f. Solid phases such as anorthite, tridymite, pseudowollastonite and gehlenite can be seen in equilibrium with liquid. An example of complete liquid phase is shown in Fig. 3a indicating the typical microstructure of a slag equilibrated above the liquidus temperature for this slag composition. Figure 3b shows anorthite primary phase in equilibrium with liquid for the sample S205B equilibrated at 1230 °C. Here anorthite is the primary phase for this slag composition and the liquidus temperature is bracketed between 1230 and 1245 °C. The composition of the S200 master slag lies within the anorthite primary phase field and the liquidus is predicted to be 1340 °C based on the phase diagram of Rankin and Wright [44]. Upon addition of ~ 5% B_2O_3, the primary phase field does not change but the liquidus temperature was reduced by approximately 100–110 °C. For the same composition, at lower temperatures, two solid phases (anorthite and pseudowollastonite) were in equilibrium with liquid as shown in Fig. 3c. For some compositions, tridymite was also found in equilibrium with anorthite and liquid at a significantly lower temperature than the liquidus of the slag. Such an example can be represented by Fig. 3d for S110B slag quenched from 1050 °C. Primary gehlenite phase in equilibrium with liquid was observed in the boron-free master slag (S300) composition at 1310 °C is shown in Fig. 3e which agrees with the ternary $CaO–Al_2O_3–SiO_2$ phase diagram [44]. Unlike anorthite in the S100 and S200 series slags, the addition of boron to the S300 master slag changes the primary phase from gehlenite to pseudowollastonite as shown in Fig. 3f, where the pseudowollastonite primary phase is now in equilibrium with the liquid. It is to be noted that the chemical composition of anorthite is close to the composition of the equilibrium liquid phase in the S100 series of slags, therefore both phases share a similar contrast in BSE imaging and require a careful adjustment in brightness and contrast to distinguish the anorthite primary phase and the liquid matrix. This can be observed in Fig. 3d. For the low-boron doped slags (S305B and S310B), pseudowollastonite crystals were in equilibrium with their liquid at close to their liquidus temperature. As the BSE images show, the brighter pseudowollastonite crystals form in different shapes and sizes in close association with the relatively darker contrast anorthite phase (Fig. 3d). Anorthite in the S200 and S300 series samples appears relatively darker in contrast as opposed to the S100 series. This is due to the comparatively higher CaO content in the liquid phase appearing brighter in the BSE imaging conditions of the SEM. On the other hand, pseudowollastonite, having higher Ca content, appears brighter in backscatter images since Ca is the heaviest element present.

Liquidus Temperature of the Slags

The liquidus temperatures of the 3 master slags and 12 sub-slags containing different boron contents are shown in Figs. 4, 5, 6. For the S100 (C/S = 0.3) slag series, the

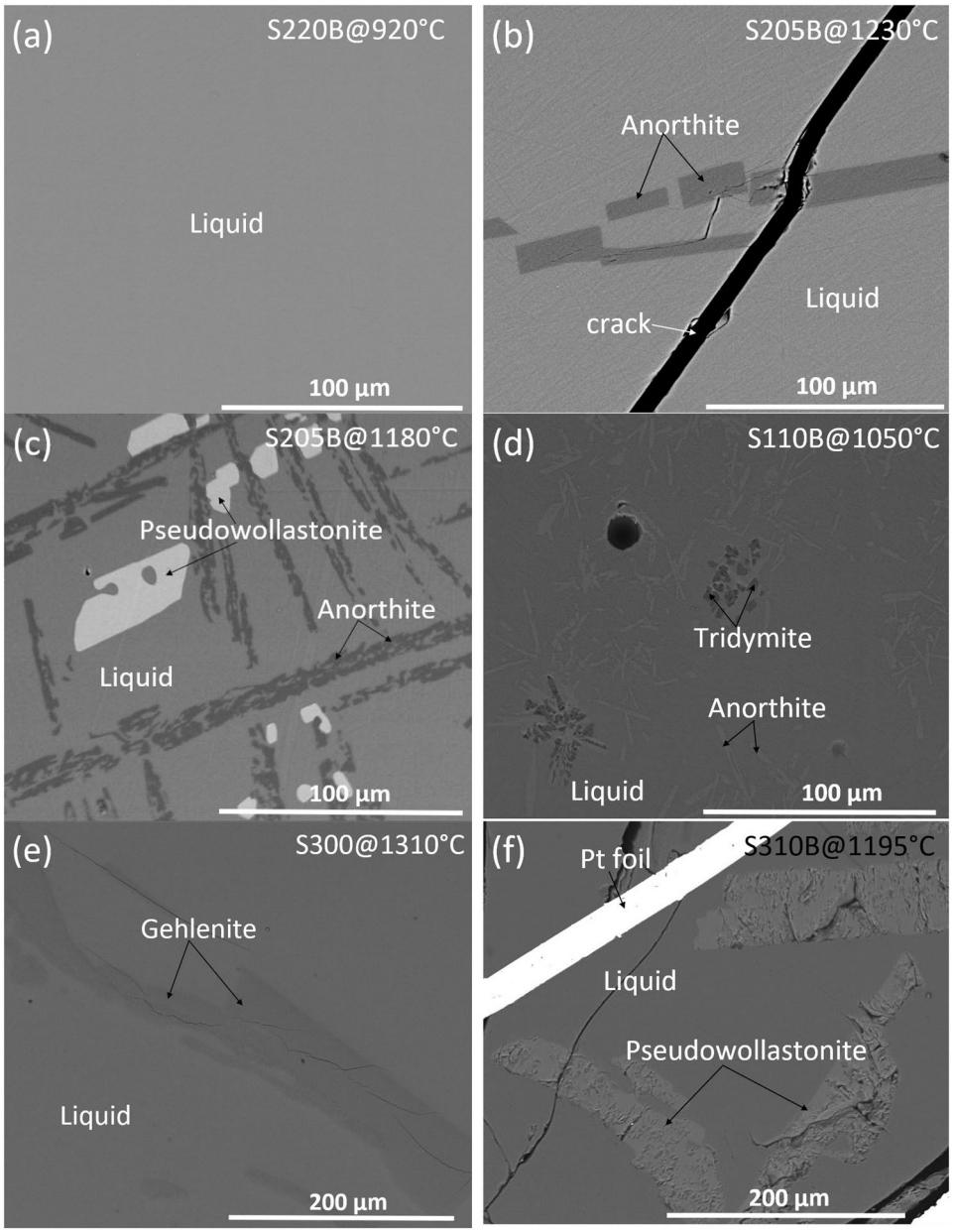

Fig. 3 Representative micrographs of S100 series of quenched slags **a** Liquid of S220B slag at 920 °C **b** Anorthite of S205B slag at 1230 °C **c** Anorthite + Pseudowollastonite + Liquid of S205B slag at 1180 °C **d** Anorthite + Tridymite + Liquid of S110B slag at 1050 °C **e** Gehlenite + Liquid of S300 at 1310 °C and **f** Pseudowollastonite + Liquid of S310B at 1195 °C

liquidus temperatures are plotted in Fig. 4. Results show that the liquidus temperature of 1320 ± 15 °C determined for the B-free master slag was in good agreement with the 1345 °C liquidus temperature reported by Rankin and Wright [44]. Upon progressive addition of B_2O_3 to the master slag, the liquidus temperature dropped significantly. With 5.2 wt% addition of B_2O_3 (S105B composition), at 1180 ± 20 °C anorthite was observed in equilibrium with liquid, while at 1200 °C the sample contained only liquid phase. This indicates that a temperature of 1200 °C is above the liquidus of the slag while 1180 °C is below the liquidus temperature. Therefore, the liquidus for the S105B slag was bracketed between 1180 and 1200 °C with an uncertainty of 20 °C. This represents a lowering of the liquidus temperature by around 140 °C compared to the B-free master slag composition. An increase in the boron content to 9.2 wt% (S110) reduced the liquidus temperature further to 1100 ± 20 °C. This trend continued with higher boron contents with compositions S115B and S120B having liquidus temperatures of 1040 ± 10 °C and 1035 ± 10 °C respectively. In all samples, the primary phase coexisting with a liquid below the liquidus temperature was anorthite. Although an increase in the amount of B_2O_3 consistently decreased the liquidus temperature of C/S = 0.3 master slag, the amount by which the temperature was lowered, decreased with increasing boron content. The liquidus lowering effect was greater for boron contents between 5 and 10 wt% while at the higher boron contents (i.e. from above 10–19 wt%), the extent of

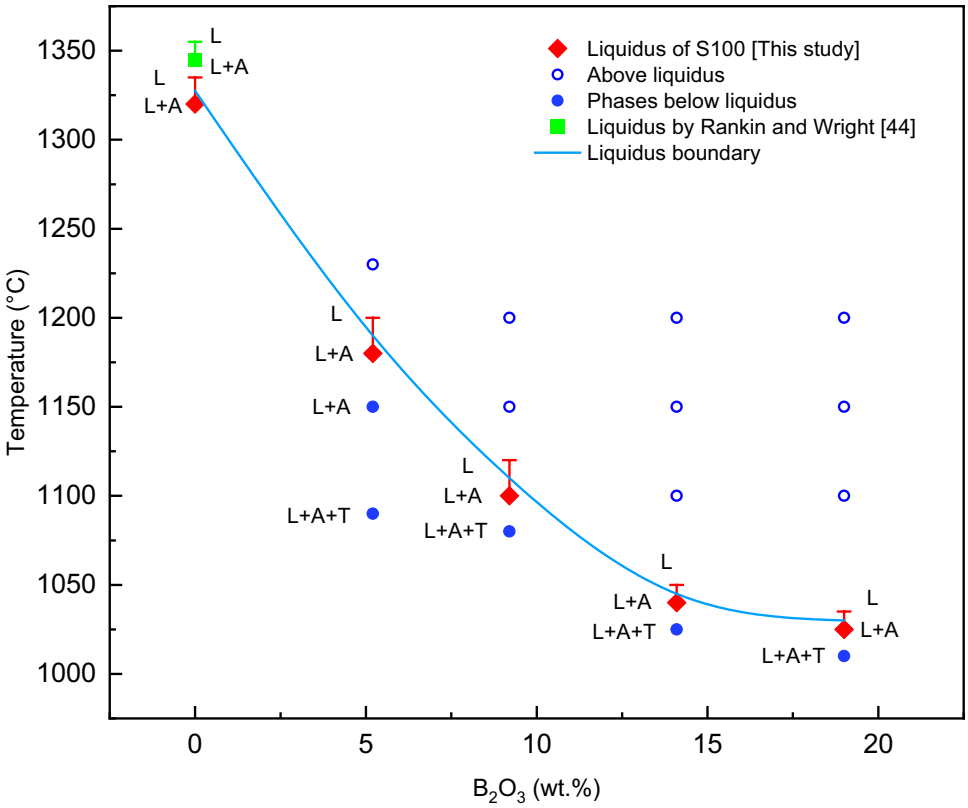

Fig. 4 Liquidus temperatures of the S100B series of slags doped with varying B_2O_3 contents; C/S = 0.3 and 15.6–18.2 wt% Al_2O_3. Error bar indicates the liquidus uncertainty range; *L* Liquid, *A* Anorthite, *T* Tridymite

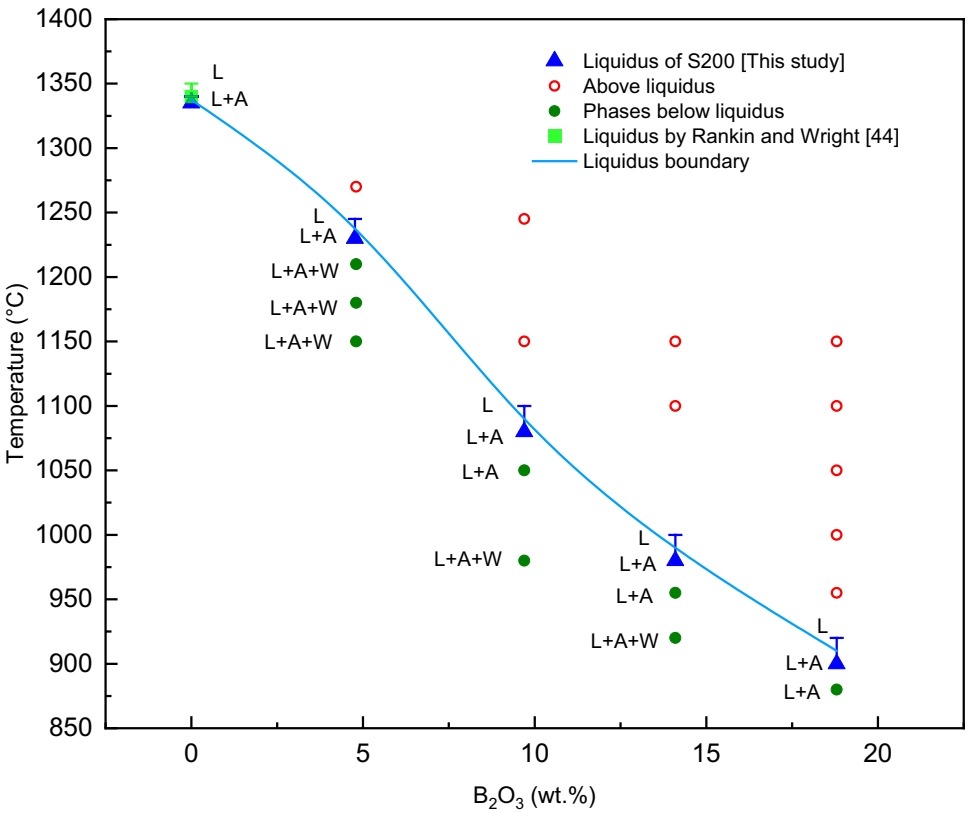

Fig. 5 Liquidus temperatures of the S200B series of slags doped with varying B_2O_3 contents; C/S = 0.6 and 15.8–18.5 wt% Al_2O_3. Error bar indicates the liquidus uncertainty range; *L* Liquid, *A* Anorthite, *W* Pseudowollastonite

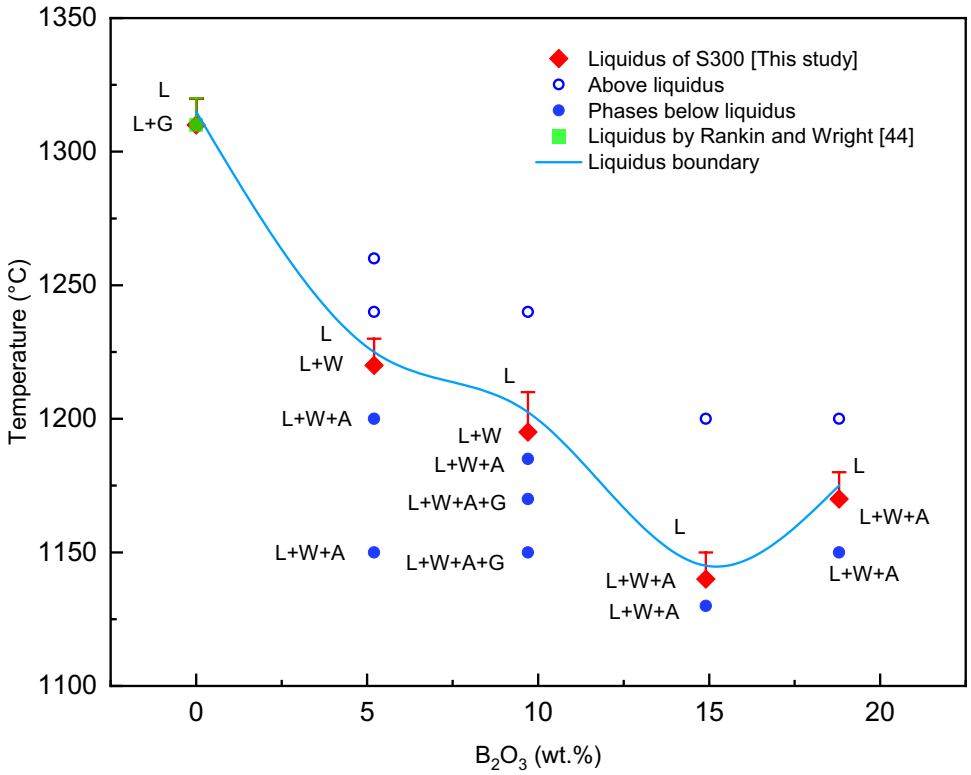

Fig. 6 Liquidus temperatures of the S300B series slags doped with varying B_2O_3 contents; C/S = 1.0 and 15.6–18.2 wt% Al_2O_3. Error bar indicates the liquidus uncertainty range; *L* Liquid, *A* Anorthite, *W* Pseudowollastonite, *G* Gehlenite

liquidus reduction is comparatively less steep. At 14 wt% B_2O_3 the liquidus was 1040 ± 10 °C and with further B_2O_3 addition up to 19 wt% the liquidus was reduced further by only 15–1025 ± 10 °C. Thus, the lowest liquidus for the S100 (C/S = 0.3) series slags was 1025 ± 10 °C which indicates a total lowering of liquidus by around 300 °C when fluxed with 19 wt% B_2O_3 doping.

For the S200 (C/S = 0.6) slag series, the liquidus temperatures are plotted in Fig. 5. The boron-free ternary CAS master slag for this composition has a liquidus temperature of 1335 °C. As for the C/S = 0.3 slag series, increasing the B_2O_3 content caused a significant reduction in the liquidus temperature. At the lowest boron content (S205B, 4.8 wt% B_2O_3), the slag was a completely liquid phase at 1245 °C while at 1230 °C the slag showed anorthite in equilibrium with liquid. Thus, the liquidus temperature for S205B slag was between 1230 and 1245 °C with 15 °C uncertainty. With a further increase in the amount of B_2O_3 added, the liquidus temperature dropped to 1080 °C with 9.7 wt% B_2O_3, 980 °C with 14.1 wt% B_2O_3 and 900 °C with 18.8 wt% B_2O_3. In each sample, at temperatures below the liquidus, anorthite was the only primary phase in equilibrium with the liquid. Unlike the S100 slag series however, a linear decline in the slag liquidus temperature was evident upon increasing B_2O_3 content with the lowest liquidus temperature determined for sample S220B as 900 ± 20 °C. Thus, the S200 series slags (C/S = 0.6) showed a decrease of the liquidus by more than 400 °C from that of the boron-free CAS master slag when doped by 18.8 wt% B_2O_3. Further experiments are required to determine if the trend continues at higher levels of B_2O_3 doping.

Figure 6 shows the experimentally obtained liquidus temperatures for the slag series S300 having a C/S ratio of 1.0 and with increasing B_2O_3 in the quaternary slags. According to the ternary CAS phase diagram the liquidus for the master slag S300 was estimated as 1310 °C and was located in the gehlenite primary phase field [44], although it should be noted that the composition is in close proximity to the gehlenite-anorthite-pseudowollastonite ternary eutectic. Overall, this slag series experienced significant lowering of the liquidus temperature with increasing B_2O_3 content in slags containing up to 14.9 wt% B_2O_3 after which the liquidus began to rise when the B_2O_3 content rose above this level. Addition of 5.2 wt% B_2O_3 (S305) caused a reduction in the liquidus temperature to 1220 °C, while additions of 9.7 wt% and 14.9 wt% saw the liquidus reduce even further to 1195 °C and 1140 °C, respectively. With the further addition of B_2O_3 to 18.8 wt% the liquidus increased to 1170 °C for slag S320B. For the S300 B-doped series therefore, the lowest liquidus temperature was 1140 °C with 14.9 wt% B_2O_3 representing an overall 170 °C decline in the slag liquidus due to the B-doping. In contrast to the S100 and S200 series, the addition of increased amounts of boron caused a shift in the primary phase assemblage. In the samples with boron levels of less than 10 wt% the primary crystalline phase switched from gehlenite (in the B-free system) to that

of pseudowollastonite indicating that the ternary eutectic had shifted due to the presence of boron causing an expansion of the pseudowollastonite primary phase field. A further increase in the B content (i.e., 14.9 and 18.8 wt%) saw the appearance of anorthite and wollastonite coexisting with the liquid probably because of the expansion of pseudowollastonite and anorthite primary phase field in the quaternary slag system resulting from the doping with B_2O_3.In the ternary CAS system this equilibrium could be represented by the phase boundary between pseudowollastonite and anorthite primary phases. It is seen that liquidus temperature increases with increasing B_2O_3 above 14.9 wt% while there is no change in the phase assemblage (Fig. 6). This can happen when the equilibrium composition falls in the cotectic curve between pseudowollastonite and anorthite primary phase field along which these two solid phases are in equilibrium with the liquid in the pseudoternary $CaO–Al_2O_3–SiO_2$ slag system doped with B_2O_3. When B_2O_3 content increases and proportionally the other components decrease the equilibrium liquid composition reaches the highest temperature point on the cotectic boundary which is indicated by the intersecting point on the cotectic curve by the anorthite–gehlenite–pseudowollastonite compatibility triangle.

The results from the three slag series examined have shown that doping with B_2O_3 reduces the slag liquidus significantly, but the reduction in temperature varies according to the composition of the initial master slag (C/S ratio) and the primary phase field that can be seen from the liquidus trend in Figs. 4, 5, 6. The liquidus reduction is linear when the primary phase was anorthite and did not change with progressive B-doping within the master slags (C/S = 0.3–0.6) although for C/S = 0.3 the trend reached a plateau beyond 14.1 wt% B_2O_3. However, for the master slag having a C/S = 1.0 upon B_2O_3 doping the primary phase field changes from gehlenite to pseudowollastonite and eventually falls on the boundary between pseudowollastonite and anorthite having these solid phases in equilibrium with the liquid. These phase transitions cause the non-linear changes in the liquidus temperatures of this series of slags. Among the three slags series, the S300 series showed the least effect of boron in lowering the liquidus temperature. In contrast, the highest reduction in liquidus temperature was in S200 series slags with an overall 435 °C reduction in the liquidus (composition S220B) while the S100 series experienced a maximum decline of 295 °C (composition S120B). Similar findings regarding the effect of boron on liquidus temperatures have been reported by other researchers where the effect of adding boron to a CAS-MgO slag was investigated using a similar technique of high temperature equilibration and drop-quench followed by EPMA [32]. They showed that the liquidus temperature dropped by 136 °C when doped with 4.9 wt% B_2O_3 in a slag with a C/S of ratio 1.1, and 8 wt% MgO and 16 wt% Al_2O_3.

Effect of C/S Ratio on the Liquidus Temperature of Slags

A comparison of the effect of C/S ratio on the liquidus temperature of B-doped slags shows that at lower B_2O_3 contents (5.0–9.5 wt%), for a given B_2O_3 content, the liquidus temperature increases slightly with increasing C/S ratio (Fig. 7). An overall increase of 40 °C was noted for the change of C/S ratio from 0.3 to 1.0 at 5 wt% B_2O_3 while at the increased B_2O_3 content (9.5 wt%) the liquidus temperature rose by 105 °C from 1080 °C for C/S ratio 0.3 to 1185 °C for C/S ratio 1.0. In contrast, at higher B_2O_3 contents (14 and 19 wt%), the liquidus initially began to reduce between C/S ratios 0.3 and 0.6 before sharply rising at C/S = 1.0 forming a V-shape pattern of the liquidus variation (Fig. 7). From the liquidus of samples with C/S ratio = 1.0 for 14.9 wt% and 18.8 wt% it is seen that increasing B_2O_3 content with this composition of slags increases the liquidus. A comparative analysis of the results showed that the best effect of reducing liquidus temperature with B_2O_3 doping was obtained in the S200 slag series with C/S ratio 0.6 while the S100 series (C/S = 0.3) also showed significant reduction of the slag liquidus. On the other hand, for the S300 slag series (C/S = 1.0), liquidus temperatures decreased at the lower boron contents but increased again beyond 14 wt% B_2O_3. Also, the degree of liquidus lowering in the C/S = 1.0 slags was smaller compared to the other two slag series. This suggests the optimum C/S ratio is 0.6. Similar results were found for $CaO–Al_2O_3–SiO_2–Na_2O$ system where a sharp increase in the liquidus was observed with Na_2O contents above 9 wt% in larnite primary phase field [42]. The results indicate, therefore, that within the investigated slag compositions the S200 slag series would be the best to flux with B_2O_3 to obtain relatively lower practicable liquidus temperatures. The optimum composition would be S220B with a C/S ratio of 0.6 and 18.3 wt% B_2O_3 which would result in a liquidus temperature of 920 ± 20 °C.

Comparison with CAS-Na_2O Slags

In a recent study [42], the effect of Na_2O on the liquidus temperature in CAS slags was studied. Overall, the addition of B_2O_3 was found to be more effective in lowering the liquidus temperature of CAS slags compared to the similar amount of Na_2O as can be seen in Fig. 8. The largest decline in the liquidus temperature with boron doping was 435 °C for the S200 slag series (C/S = 0.6) while for the Na_2O doped slags the maximum reduction of liquidus was reported as 225 °C within the same master slag. For the S100 (C/S = 0.3) composition, the maximum reduction in liquidus temperature caused by B_2O_3 doping was 285 °C while it was only 150 °C for Na_2O doping. On the contrary, for the S300 series, the liquidus decreased by 170 °C to

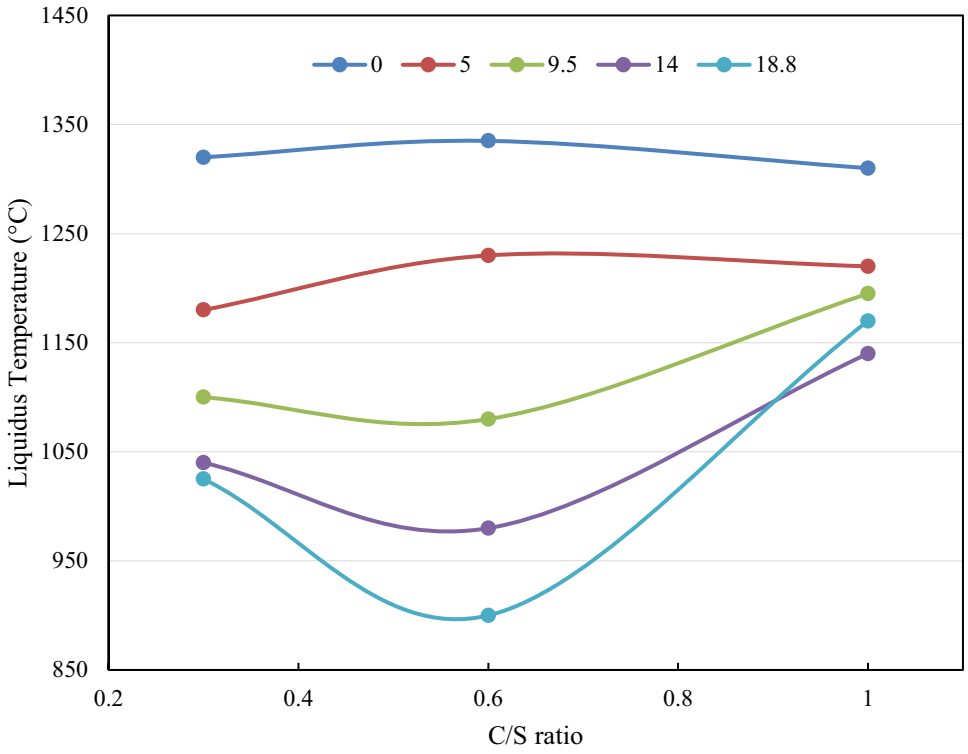

Fig. 7 Variation of the liquidus temperature with C/S ratio for the different B_2O_3 contents (wt%) in the slags

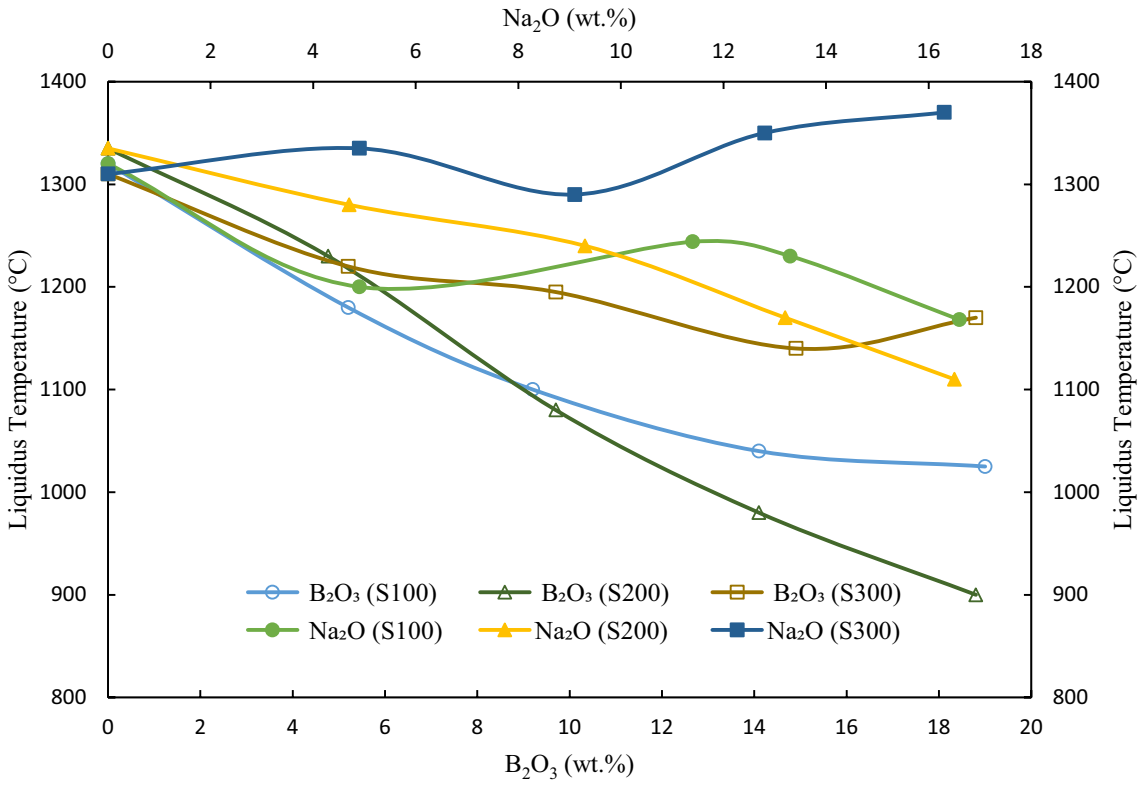

Fig. 8 Comparison of the effect of B_2O_3 with Na_2O on the liquidus temperature for CAS slags. The Na and B-free slag liquidus temperatures were taken from Rankin and Wright [44]

1140 °C with 14.6 wt% B_2O_3 and increased to 1170 °C at 18.8 wt% B_2O_3. In general, adding Na_2O in the CAS slag lowers the liquidus in the quaternary CAS–Na_2O slags in a like manner to the CAS–B_2O_3 system. However, Na_2O levels above 9 wt% increased the liquidus of S300 (C/S = 1) slags. A similar pattern was observed for the same series of slags above 14.6 wt% B_2O_3. A sharp fall in the liquidus temperature was observed in Na_2O containing slag series due to the primary phase field changes, which was not seen in the CAS–B_2O_3 slags. The greater extent of liquidus reduction in blast furnace slags by B_2O_3 compared to Na_2O was also reported by Chen et al. [32] which agrees with the findings of this current study.

While in the S100 and S200 master slags the progressive doping by Na_2O changed the primary phase field from anorthite (Na-free slag) to pseudowollastonite, in the B_2O_3 doped system adding a similar flux content did not change the phase assemblages from that of the boron-free master slags. On the other hand, Na_2O doping of the S300 (C/S = 1.0) composition changed the primary phase from gehlenite to larnite, while boron doping changed the phase assemblage to anorthite and pseudowollastonite in equilibrium with liquid. Within a very narrow temperature bracket the two solid phases remain in equilibrium with liquid. Therefore, it was difficult to ascertain which one is the primary phase in this case. The equilibration experiments were repeated several times to ensure the reproducibility of the results. Every time the same phase assemblages were obtained.

Application of the Liquidus and Phase Equilibria Data

The experimentally determined liquidus temperature and phase equilibria data of slags in the CAS–B_2O_3 system can be used to design smelting operations to recover various metals from e-waste materials. This study has determined the liquidus temperature of 15 slags relevant to the composition of slag generated in electronic PCBs smelting. One of the objectives of boron doping in CAS slag was to lower the liquidus temperature of the highly refractory oxide CAS system. Overall, this objective was achieved as results indicated it was possible to lower the liquidus by more than 400 °C by B_2O_3 doping. However, the degree of reduction in the liquidus temperature was not the same for all the slags examined, being highest in slag S200 series with a C/S ratio of 0.6 and with doping by 18.8 wt% B_2O_3. In contrast, for some slags and at higher B_2O_3 on the slags the liquidus temperature increased with the increasing B_2O_3 flux content. Therefore, the precise liquidus data presented in this study will play important role to identify the best slag and flux composition based on the feed materials' compositions. The experimental findings of the liquidus will guide the selection of the optimum slag compositions required to obtain the lowest practicable liquidus temperature. This will in turn reduce the energy required to recover valuable metals from e-wastes and bring operational flexibility. In addition, this information will be useful in modelling more complex slags using thermochemical calculation packages.

Conclusion

Phase equilibria of the quaternary system CaO–Al_2O_3–SiO_2–B_2O_3 was studied to investigate the effect of B_2O_3 on the liquidus temperature in slag compositions with C/S ratios of 0.3–1.0 and 15.6–19.1 wt% Al_2O_3. The phase assemblages of the slags were identified at or close to their respective liquidus temperature, and the equilibrium phase composition was precisely determined with EPMA. Anorthite, pseudowollastonite, gehlenite and tridymite solid phases were found in equilibrium with liquid. An iterative approach was followed to estimate the liquidus temperature of slags within an error between 10 to 20 °C. Overall, doping with B_2O_3 decreased the liquidus temperature relative to the boron-free CaO–Al_2O_3–SiO_2 based master slags but an increase in case of C/S ratio 1.0 at higher B_2O_3 doping. The highest degree of liquidus reduction was obtained in the slags with C/S ratio 0.6 and with increasing B_2O_3. A decline of liquidus by 435 °C was obtained with 18.8 wt% B_2O_3 doping in S220 slag. The lowest liquidus temperature within the investigated slags was 900 °C while the same undoped boron-free slag had the liquidus of 1335 °C. In contrast, the liquidus increased due to increasing B_2O_3 doping in S300 (C/S = 1.0) series slags at higher boron content. A comparison with similar Na_2O doping in the CAS slag shows boron has a more pronounced effect in lowering the slag liquidus. Based on the liquidus temperature determined in this research CAS-B slags could be used in smelting waste PCBs at lower operating temperatures and B_2O_3 can be considered as flux to reduce the liquidus with C/S ratio 0.3 and 0.6. However, it might not be helpful to use B_2O_3 when the slag composition is close to C/S ratio 1.0.

Appendix: Equilibrium Phase Composition

The phase equilibria study of the quaternary CaO–Al_2O_3–SiO_2–B_2O_3 system identified several solid phases including anorthite, tridymite, pseudowollastonite and gehlenite in equilibrium with liquid at temperatures just below the predicted liquidus. The chemistry of the different phase assemblages and liquids were quantified using EPMA with the average equilibrium composition of the phases provided in Table 2. Note, for B-doped slags the composition of phases at the bracketed liquidus temperature and at the lowest experimental temperature

Table 2 Equilibrium phase compositions determined by EPMA

Sample ID	Temperature (°C)	Time (hours)	Phases	Composition (wt%)			
				B_2O_3	SiO_2	CaO	Al_2O_3
S100	1320	22	Liquid	0.0	61.3 (0.2)	20.4 (0.1)	18.2 (0.0)
			Anorthite	0.0	44.5 (0.4)	20.3 (0.3)	35.1 (0.4)
S105B	1180	4	Liquid	5.0 (0.9)	58.2 (0.8)	19.6 (0.2)	17.1 (0.6)
			Anorthite	1.1 (0.5)	44.7 (0.7)	20.0 (0.1)	34.1 (1.5)
S105B	1090	4	Liquid	6.2 (0.9)	58.7 (1.3)	20.6 (0.7)	14.3 (0.3)
			Anorthite	0.7 (0.4)	45.2 (1.5)	19.6 (0.0)	34.8 (1.0)
			Tridymite	0.9 (0.4)	98.1 (0.3)	0.4 (0.0)	0.6 (0.0)
S110B	1100	4	Liquid	7.7 (1.7)	56.3 (0.6)	18.7 (0.1)	17.1 (0.1)
			Anorthite	0.4 (0.2)	44.5 (0.7)	19.4 (0.2)	35.6 (0.9)
S110B	1050	4	Liquid	10.0 (1.2)	55.2 (0.8)	19.3 (0.3)	15.3 (0.3)
			Anorthite	1.2 (0.5)	44.5 (0.6)	19.9 (0.2)	34.1 (1.1)
			Tridymite	0.5 (0.2)	98.2 (0.5)	0.3 (0.0)	0.5 (0.1)
S115B	1043	4	Liquid	12.2 (1.3)	54.1 (0.4)	17.4 (0.3)	16.2 (0.4)
			Anorthite	1.5 (1.1)	45.4 (1.6)	20.0 (0.7)	33.9 (1.0)
S115B	1000	4	Liquid	12.2 (1.3)	53.0 (0.7)	18.4 (0.6)	16.2 (0.2)
			Anorthite	1.2 (0.5)	45.0 (0.8)	19.5 (0.2)	34.1 (0.4)
			Tridymite	1.4 (0.8)	97.5 (0.5)	0.4 (0.0)	0.6 (0.1)
S120B	1035	4	Liquid	16.0 (1.3)	51.8 (1.1)	16.5 (0.2)	15.6 (0.2)
			Anorthite	0.6 (0.2)	45.2 (0.5)	20.0 (0.2)	34.7 (0.6)
S120B	1000	4	Liquid	16.4 (1.6)	51.2 (1.2)	16.8 (0.2)	15.4 (0.3)
			Anorthite	1.2 (0.5)	45.0 (0.8)	19.5 (0.2)	34.1 (0.4)
			Tridymite	1.1 (0.8)	97.7 (0.4)	0.4 (0.0)	0.6 (0.1)
S200	1335	24	Liquid	0.0	51.4 (0.1)	30.3 (0.1)	18.1 (0.1)
			Anorthite	0.0	44.0 (0.5)	20.2 (0.3)	35.6 (0.4)
S205B	1230	4	Liquid	4.7 (1.0)	48.5 (0.1)	29.2 (0.0)	17.4 (0.1)
			Anorthite	0.8 (0.1)	44.8 (0.1)	19.4 (0.0)	34.8 (0.1)
S205B	1150	4	Liquid	4.8 (0.8)	50.5 (0.2)	27.9 (0.1)	16.7 (0.2)
			Anorthite	0.6 (0.2)	44.2 (0.3)	19.7 (0.2)	35.3 (0.3)
			Pseudowollastonite	0.3 (0.2)	51.6 (0.3)	47.6 (0.4)	0.3 (0.1)
S210B	1080	4	Liquid	9.9 (0.5)	46.8 (0.28)	28.7 (0.0)	14.5 (0.0)
			Anorthite	1.3 (0.9)	45.2 (0.7)	21.0 (0.8)	32.3 (1.4)
S210B	980	4	Liquid	12.4 (1.2)	46.5 (0.5)	26.7 (0.3)	14.2 (0.3)
			Anorthite	0.6 (0.3)	43.0 (0.4)	20.5 (0.8)	35.7 (0.4)
			Pseudowollastonite	0.9 (0.5)	51.5 (0.1)	46.7 (0.0)	1.2 (0.0)
S215B	980	4	Liquid	13.5 (1.2)	44.5 (0.4)	26.8 (0.1)	15.0 (0.4)
			Anorthite	1.0 (0.5)	46.6 (0.7)	19.5 (0.3)	32.7 (0.6)
S215B	920	4	Liquid	14.0 (1.2)	45.0 (0.3)	26.4 (0.4)	14.4 (1.0)
			Anorthite	2.8 (1.8)	46.7 (0.5)	20.4 (0.7)	29.9 (1.2)
			Pseudowollastonite	0.6 (0.3)	51.4 (0.1)	47.8 (0.2)	0.1 (0.0)
S220B	900	8	Liquid	17.6 (1.2)	42.0 (0.5)	24.8 (0.2)	15.4 (0.1)
			Anorthite	1.4 (0.3)	42.3 (0.7)	20.2 (0.2)	35.8 (0.4)
S220B	860	8	Liquid	16.7 (0.9)	42.8 (0.5)	24.9 (0.1)	15.4 (0.2)
			Anorthite	0.6 (0.2)	47.1 (0.4)	19.6 (0.2)	32.4 (0.3)
S300		24	Liquid	0.0	41.4 (0.2)	40.1 (0.1)	18.4 (0.1)
			Gehlenite	0.0	23.9 (0.9)	41.5 (0.1)	34.4 (1.1)
S305B	1220	8	Liquid	4.7 (1.1)	38.6 (0.4)	38.4 (0.2)	18.0 (0.4)
			Pseudowollastonite	0.4 (0.3)	50.7 (0.4)	48.5 (0.1)	0.2 (0.2)
S305B	1150	4	Liquid	5.7 (0.8)	37.5 (0.7)	38.6 (0.3)	18.1 (0.2)
			Gehlenite	2.9 (0.4)	24.4 (0.3)	41.5 (0.2)	30.9 (0.8)

Table 2 (continued)

Sample ID	Temperature (°C)	Time (hours)	Phases	Composition (wt%)			
				B_2O_3	SiO_2	CaO	Al_2O_3
			Anorthite	1.5 (0.8)	42.5 (0.6)	20.1 (0.1)	35.7 (0.2)
			Pseudowollastonite	0.5 (0.2)	51.2 (0.7)	47.9 (0.1)	0.1 (0.0)
S310B	1195	8	Liquid	7.3 (1.8)	38.1 (0.8)	37.1 (0.6)	17.3 (0.4)
			Pseudowollastonite	0.4 (0.3)	51.4 (0.1)	47.9 (0.1)	0.1 (0.0)
S310B	1150		Liquid	9.1 (0.8)	37.2 (0.4)	36.9 (0.5)	16.6 (0.4)
			Gehlenite	1.2 (0.3)	23.1 (0.4)	41.4 (0.2)	34.1 (0.5)
			Anorthite	0.4 (0.2)	44.0 (0.5)	20.0 (0.6)	35.4 (0.7)
			Pseudowollastonite	1.4 (0.6)	49.7 (0.5)	48.3 (0.4)	0.4 (0.2)
S315B	1140	4	Liquid	9.7 (2.4)	36.3 (0.9)	36.7 (0.8)	17.2 (0.9)
			Anorthite	0.5 (0.2)	43.7 (0.4)	20.2 (0.0)	35.5 (0.3)
			Pseudowollastonite	0.4 (0.1)	51.2 (0.4)	48.2 (0.2)	0.0 (0.0)
S315B	1130	4	Liquid	10.6 (1.6)	35.6 (0.9)	36.8 (1.1)	16.8 (0.6)
			Anorthite	0.6 (0.4)	43.7 (0.1)	20.2 (0.1)	35.4 (0.0)
			Pseudowollastonite	0.6 (0.5)	50.7 (0.5)	48.4 (0.1)	0.1 (0.0)
S320B	1170	4	Liquid	16.2 (1.2)	34.6 (0.8)	33.4 (0.5)	15.6 (0.1)
			Anorthite	0.23 (0.0)	43.5 (0.3)	20.6 (0.6)	35.5 (0.6)
			Pseudowollastonite	0.5 (0.4)	51.0 (0.4)	48.0 (0.1)	0.3 (0.0)
S320B	1150	4	Liquid	15.7 (0.9)	35.8 (0.7)	37.6 (1.0)	16.6 (0.2)
			Anorthite	0.4 (0.2)	42.9 (0.2)	21.5 (0.5)	35.0 (0.4)
			Pseudowollastonite	0.7 (0.4)	50.3 (0.5)	48.3 (0.3)	0.5 (0.0)

*The number within the brackets indicates the standard deviation of the analysis points

with multiple solid phases are mentioned. The test runs in between these were used as the steps of iterative approach and are not included in this table to keep it concise.

With a 5 µm defocus, it was not possible to get an accurate compositional analysis of the tridymite phase which was often less than 5 µm in grain size. Therefore, when analysing the fine grained tridymite phase, the electron beam spot was highly focused to provide an analysis volume of ~ 1 μm^3. Compared to analysis data for the heavier elements Ca, Al and Si, higher standard deviations were noted when analysing for boron. Although additional precautions were taken when analysing boron (see EPMA section above) the analysis remains challenging and as consequence a higher standard deviation in the boron content of both liquid and solid phases was common. In general, boron was incompatible with most crystalline phases and tended to concentrate in the liquid phase.

Acknowledgements The authors are grateful to Tom Austin and the Materials Characterization Team of CSIRO Mineral resources for their support to run the experiments and analyze the samples. Also, the support of RMIT Microscopy and Microanalysis is acknowledged by the authors for their support in using SEM. The authors also acknowledge the financial support jointly provided by CSIRO and RMIT University.

Declarations

Conflict of interest All authors declare that they have no conflict of interest.

References

1. RSC (2022) https://www.rsc.org/new-perspectives/sustainability/elements-in-danger/. Accessed 02 Feb 2022
2. Forti V, Balde CP, Kuehr R, Bel G (2020) The global e-waste monitor 2020: quantities, flows and the circular economy potential. https://collections.unu.edu/view/UNU:7737. Accessed 26 Mar 2021
3. Cesaro A, Marra A, Kuchta K, Belgıorno V, Van HED (2018) WEEE management in a circular economy perspective: an overview. Glob Nest J 20:743–750
4. Cui J, Zhang L (2008) Metallurgical recovery of metals from electronic waste: a review. J Hazard Mater 158:228–256
5. Van YJ, Boxall NJ, Cheng KY, Nikoloski AN, Moheimani NR, Kaksonen AH (2021) E-waste recycling and resource recovery: a review on technologies, barriers and enablers with a focus on oceania. Metals 11:1313–1353
6. Chen J, Wang Z, Wu Y, Li L, Li B, Pan DA, Zuo T (2019) Environmental benefits of secondary copper from primary copper based on life cycle assessment in China. Resour Conserv Recycl 146:35–44

7. Abdelbasir SM, El-Sheltawy CT, Abdo DM (2018) Green processes for electronic waste recycling: a review. J Sustain Metall 4:295–311
8. Golev A, Corder GD, Rhamdhani MA (2019) Estimating flows and metal recovery values of waste printed circuit boards in Australian e-waste. Miner Eng 137:171–176
9. Islam MK, Haque N, Somerville M, Pownceby MI, Bhargava S, Tardio J (2022) Estimation of the generation and value recovery from e-waste printed circuit boards: Bangladesh case study. In: REWAS 2022: developing tomorrow's technical cycles, vol I. Springer, Cham, pp 91–102
10. Wan X, Kleemola L, Klemettinen L, O'Brien H, Taskinen P, Jokilaakso A (2021) On the kinetic behavior of recycling precious metals (Au, Ag, Pt, and Pd) through copper smelting process. J Sustain Metall 7:920–931
11. Park HS, Kim YJ (2019) A novel process of extracting precious metals from waste printed circuit boards: utilization of gold concentrate as a fluxing material. J Hazard Mater 365:659–664
12. Gu F, Summers PA, Hall P (2019) Recovering materials from waste mobile phones: recent technological developments. J Cleaner Prod 237:117657
13. Li K, Xu Z (2019) A review of current progress of supercritical fluid technologies for e-waste treatment. J Cleaner Prod 227:794–809
14. Mir S, Dhawan N (2022) A comprehensive review on the recycling of discarded printed circuit boards for resource recovery. Resour Conserv Recycl 178:106027
15. Anindya A (2012) Minor elements distribution during the smelting of WEEE with copper scrap. PhD Thesis, RMIT University
16. Islam MK, Haque N, Somerville MA (2021) Characterisation and techno-economics of a process to recover value from e-waste materials. TMS 2021 150th Annual Meeting & Exhibition Supplemental Proceedings. Springer, Cham, pp 995–1006
17. Park HS, Han YS, Park JH (2019) Massive recycling of waste mobile phones: pyrolysis, physical treatment, and pyrometallurgical processing of insoluble residue. ACS Sustain Chem Eng 7:14119–14125
18. Ogunniyi IO, Vermaak MKG, Groot DR (2009) Chemical composition and liberation characterization of printed circuit board comminution fines for beneficiation investigations. Waste Manage 29:2140–2146
19. Jak E, Hayes PC (2008) Phase equilibria determination in complex slag systems. Miner Process Extr Metall 117:1–17
20. Henao HM, Nexhip C, George-Kennedy DP, Hayes PC, Jak E (2010) Investigation of liquidus temperatures and phase equilibria of copper smelting slags in the FeO–Fe_2O_3–SiO_2–CaO–MgO–Al_2O_3 system at PO_2 10 (-8) atm. Metall Mater Trans B 41:767–779
21. Park H-S, Park SS, Sohn I (2011) The viscous behavior of FeO_t–Al_2O_3–SiO_2 copper smelting slags. Metall Mater Trans B 42:692–699
22. Zhao BJ, Hayes PC, Jak E (2011) Effects of Al_2O_3 and CaO/SiO_2 ratio on phase equilibria in the ZnO–FeO–Al_2O_3–CaO–SiO_2 system in equilibrium with metallic iron. Metall Mater Trans B 42:50–67
23. Kim H, Kim WH, Park JH, Min DJ (2010) A study on the effect of Na_2O on the viscosity for ironmaking slags. Steel Res Int 81:17–24
24. Ma XD, Wang G, Wu SL, Zhu JM, Zha BJ (2015) Phase equilibria in the CaO–SiO_2–Al_2O_3–MgO system with CaO/SiO_2 ratio of 1.3 relevant to iron blast furnace slags. ISIJ Int 55:2310–2317
25. Wang L, Zhang J, Sasaki Y, Ostrovski O, Zhang C, Cai D (2017) Stability of fluorine-free CaO–SiO_2–Al_2O_3–B_2O_3–Na_2O mold fluxes. Metall Mater Trans B 48:1055–1063
26. Ma J, Li W, Fu G, Zhu M (2021) Effect of B_2O_3 on the melting temperature and viscosity of CaO–SiO_2–MgO–Al_2O_3–TiO_2–Cr_2O_3 slag. J Sustain Metall 7:1190–1199
27. Abel BM, Mauro JC, Smedskjaer MM, Morgan JM, LaPierre CL, Swan GR, Mack ME, Ellison AJ (2013) Liquidus surface of MgO–CaO–Al_2O_3–SiO_2 glass-forming systems. J Non-Cryst Solids 363:39–45
28. Heo JH, Cho J-W, Park HS, Park JH (2019) Crystallization and vitrification behavior of CaO-SiO_2-FeO_t-Al_2O_3 slag: fundamentals to use mineral wastes in production of glass ball. J Cleaner Prod 225:743–754
29. Chen X-d, Kong L-x, Bai J, Bai Z-q, Li W (2016) Effect of Na_2O on mineral transformation of coal ash under high temperature gasification condition. J Fuel Chem Technol 44:263–272
30. Dai X, Bai J, Li D-t, Yuan P, Yan T-g, Kong L-x, Li W (2019) Experimental and theoretical investigation on relationship between structures of coal ash and its fusibility for Al_2O_3–SiO_2–CaO–FeO system. J Fuel Chem Technol 47:641–648
31. Yan T, Bai J, Kong L, Li H, Wang Z, Bai Z, Zhao H, Li W (2019) Improved prediction of critical-viscosity temperature by fusion behavior of coal ash. Fuel 253:1521–1530
32. Chen M, Zhang W, Zhao Z, Evans T, Zhao B (2016) Effects of minor elements to the liquidus temperatures of blast furnace slags. ISIJ Int 56:2156–2160
33. Akberdin AA, Kim AS, Sultangaziev RB (2021) Surface tension of melts of CaO–SiO_2–Al_2O_3–B_2O_3 system. Steel Transl 51:15–21
34. Yang J, Wang L, Wang Q, Zhang J, Sasaki Y, Zhang C, Cai D, Ostrovski O (2021) Challenges in the mold flux design: development of F-free fluxes and fluxes for casting of high-Al steel. Steel Res Int. https://doi.org/10.1002/srin.202100123
35. Kim GH, Sohn I (2019) Effect of CaF_2, B_2O_3 and the CaO/SiO_2 mass ratio on the viscosity and structure of B_2O_3-containing calcium-silicate-based melts. J Am Ceram Soc 102:6575–6590
36. Wang H, Zhang T, Zhu H, Li G, Yan Y, Wang J (2011) Effect of B_2O_3 on melting temperature, viscosity and desulfurization capacity of CaO–based refining flux. ISIJ Int 51:702–706
37. Wang Z, Shu Q, Chou K (2013) Viscosity of fluoride-free mold fluxes containing B_2O_3 and TiO_2. Steel Res Int 84:766–776
38. Fox AB, Mills KC, Lever D, Bezerra C, Valadares C, Unamuno I, Laraudogoitia JJ, Gisby J (2005) Development of fluoride-free fluxes for billet casting. ISIJ Int 45:1051
39. Wang L, Cui Y, Yang J, Zhang C, Cai D, Zhang J, Sasaki Y, Ostrovski O (2015) Melting properties and viscosity of SiO_2–CaO–Al_2O_3–B_2O_3 system. Steel Res Int 86:670–677
40. Zhang GH, Chou KC (2013) Influence of Al_2O_3/SiO_2 ratio on viscosities of CaO–Al_2O_3–SiO_2 melt. ISIJ Int 53:177–180
41. U. S. National Bureau of Standards (1975) Phase diagrams for ceramists. American Ceramic Society, Columbus, Ohio, p 630
42. Islam MK, Somerville M, Pownceby MI, Tardio J, Haque N, Bhargava S (2021) Phase equilibria study of CaO–Al_2O_3–SiO_2–Na_2O slags for smelting waste printed circuit boards. JOM 73:1889–1898
43. Rait R (1997) Phase equilibria in iron bath smelting type slags. PhD Thesis, University of Melbourne
44. Rankin GA, Wright FE (1915) The ternary system CaO-Al_2O_3-SiO_2. Am J Sci 1:1